Probing Electrostatic Interactions along the Reaction Pathway of a Glycoside Hydrolase: Histidine Characterization by NMR Spectroscopy†

Mario Schubert,‡,§ David K. Y. Poon,‡,|| Jacqueline Wicki,|| Chris A. Tarling,|| Emily M. Kwan,|| Jens E. Nielsen,⊥ Stephen G. Withers,‡,|| and Lawrence P. McIntosh*,‡,||

Department of Biochemistry and Molecular Biology, Department of Chemistry, The Michael Smith Laboratory, and The Protein Engineering Network of Centres of Excellence, University of British Columbia, Vancouver, British Columbia, Canada V6T 1Z3, and Department of Biochemistry, Conway Institute, University College Dublin, Belfield, Dublin 4, Ireland

Received February 5, 2007; Revised Manuscript Received April 17, 2007

ABSTRACT: We have characterized by NMR spectroscopy the three active site (His80, His85, and His205) and two non-active site (His107 and His114) histidines in the 34 kDa catalytic domain of *Cellulomonas fimi* xylanase Cex in its apo, noncovalently aza-sugar-inhibited, and trapped glycosyl−enzyme intermediate states. Due to protection from hydrogen exchange, the level of which increased upon inhibition, the labile $^{1}H^{\delta1}$ and $^{1}H^{\epsilon1}$ atoms of four histidines ($t_{1/2} \sim 0.1-300$ s at 30 °C and pH ~7), as well as the nitrogen-bonded protons in the xylobio-imidazole and -isofagomine inhibitors, could be observed with chemical shifts between 10.2 and 17.6 ppm. The histidine pK_a values and neutral tautomeric forms were determined from their pH-dependent $^{13}C^{\epsilon1}-^{1}H^{\epsilon1}$ chemical shifts, combined with multiple-bond $^{1}H^{\delta2/\epsilon1}-^{15}N^{\delta1/\epsilon2}$ scalar coupling patterns. Remarkably, these pK_a values span more than 8 log units such that at the pH optimum of ~6 for Cex activity, His107 and His205 are positively charged (pK_a > 10.4), His85 is neutral (pK_a < 2.8), and both His80 (pK_a = 7.9) and His114 (pK_a = 8.1) are titrating between charged and neutral states. Furthermore, upon formation of the glycosyl−enzyme intermediate, the pK_a value of His80 drops from 7.9 to <2.8, becoming neutral and accepting a hydrogen bond from an exocyclic oxygen of the bound sugar moiety. Changes in the pH-dependent activity of Cex due to mutation of His80 to an alanine confirm the importance of this interaction. The diverse ionization behaviors of the histidine residues are discussed in terms of their structural and functional roles in this model glycoside hydrolase.

Dissecting the complex network of electrostatic interactions within the folded structure of a protein remains an important experimental and theoretical challenge. In particular, understanding these interactions and their changes along the reaction pathway of an enzyme is critical for understanding the ability of active site residues and cofactors to facilitate catalysis by acting in a coordinated manner as general acids/bases, nucleophiles, and electrophiles. One method for directly interrogating the electrostatic interactions within a protein involves the measurement of the site-specific protonation states and pK_a values of its constituent ionizable groups by NMR[1] spectroscopy. This approach is particularly convenient for histidine residues, given the wealth of information that can be obtained for the ^{1}H, ^{13}C, and ^{15}N nuclei within the imidazole ring (*1*). The pK_a of an unperturbed histidine side chain also falls near the physiological pH, and thus, the ionization state of this residue can be modulated readily by its protein environment. Furthermore, histidines often play key structural roles due to the planar aromatic nature of the heterocyclic imidazole side chain, along with its ability to act not only as a hydrogen bond donor and acceptor but also as the positively charged component of a salt bridge. As such, histidine residues serve critical enzymatic roles, functioning commonly in nucleophilic and general acid/base catalysis, as well as in the chelation of metal ions.

In this study, we have characterized by NMR spectroscopy the electrostatic interactions involving the histidine residues

† This research was funded by grants from NSERC and from the Government of Canada's Network of Centres of Excellence Program, supported by the CIHR and NSERC through the Protein Engineering Network of Centres of Excellence (PENCE, Inc.). Instrument support was provided by CIHR, the Canadian Foundation for Innovation (CFI), the British Columbia Knowledge Development Fund, the UBC Blusson Fund, and the Michael Smith Foundation for Health Research. M.S. acknowledges an Alexander von Humboldt Feodor Lynen Fellowship.

* To whom correspondence should be addressed: Department of Biochemistry and Molecular Biology, Life Sciences Centre, 2350 Health Sciences Mall, University of British Columbia, Vancouver, BC, Canada V6T 1Z3. E-mail: mcintosh@chem.ubc.ca. Phone: (604) 822-3341. Fax: (604) 822-5227.

‡ Department of Biochemistry and Molecular Biology and The Michael Smith Laboratory, University of British Columbia.

§ Current address: Molecular Biology and Biophysics, ETH Zürich, 8093 Zürich, Switzerland.

|| Department of Chemistry and The Protein Engineering Network of Centres of Excellence, University of British Columbia.

⊥ University College Dublin.

[1] Abbreviations: CexCD, residues 1−315 of *C. fimi* Cex; 2FCb-CexCD, CexCD covalently modified at Glu233 with 2-deoxy-2-fluoro-β-cellobiose; HMBC, heteronuclear multiple-bond correlation; HSQC, heteronuclear single-quantum correlation; HX, hydrogen exchange; NMR, nuclear magnetic resonance; NOE, nuclear Overhauser effect; pH*, pH meter reading without correction for isotope effects; *p*NP-Cb, *p*-nitrophenyl β-cellobioside; *p*NP-Xb, *p*-nitrophenyl β-xylobioside; WT, wild type; XbIso·CexCD, CexCD noncovalently inhibited by xylobio-isofagomine; XbIm·CexCD, CexCD noncovalently inhibited by xylobio-imidazole.

10.1021/bi700249m CCC: $37.00 © 2007 American Chemical Society
Published on Web 06/05/2007

within the xylanase Cex (or CfXyn10A) from *Cellulomonas fimi*. This secreted enzyme, composed of separable N-terminal catalytic (34 kDa) and C-terminal cellulose-binding (11 kDa) domains, joined by a flexible glycosylated proline-threonine rich linker (*2*, *3*), catalyzes the cleavage of β-1,4-glycosidic bonds in xylan, as well as a range of soluble aryl glycosides based upon xylose and glucose (*4*). The catalytic domain of Cex adopts an $(\alpha/\beta)_8$-barrel structure (*5*) and is a family 10 member of the large GH-A clan of retaining glycoside hydrolases (*6*). In the retaining mechanism, a double-displacement reaction proceeds with direct nucleophilic attack upon the anomeric center of the glycone by an active site carboxylate to produce a covalent glycosyl−enzyme intermediate. A partner active site carboxyl serves a dual role of general acid and then base during the glycosylation and deglycosylation steps, respectively (*7*). Through detailed kinetic, crystallographic, and mutational studies, we and others have identified the nucleophile (Glu233) and the general acid/base catalyst (Glu127) in Cex and defined key structural and energetic determinants for substrate specificity and glycosyl−enzyme intermediate formation (*5*, *8*, *9*). These studies were facilitated by the availability of noncovalent inhibitors with micromolar to nanomolar affinities for this enzyme (*10*, *11*), as well as slow substrates, such as 2-deoxy-2-fluorocellobiosides and -xylobiosides, that form long-lived glycosyl−enzyme intermediates (*4*, *5*).

The catalytic domain of Cex (denoted as CexCD) contains five histidines, each in a distinct environment. Two of these, His107 and His114, are distant from the active site of the enzyme yet play important structural roles involving interactions with charged groups and bound water molecules. The remaining three are located in the active site of Cex, interacting with a constellation of polar groups, as well as with the bound substrate in the Michaelis complex and the glycosyl−enzyme intermediate. His85 is adjacent to the general acid/base Glu127, His205 directly contacts the nucleophile Glu233, and His80 forms a hydrogen bond to an exocyclic oxygen of the bound substrate. Using NMR spectroscopy, we demonstrate that the pK_a values of these histidines differ by at least 8 log units due to the distinct electrostatic interactions experienced by each within Cex. Furthermore, the pK_a value of His80 drops by more than 5 units upon formation of the trapped glycosyl−enzyme intermediate, illustrating the significant electrostatic changes that occur within the active site of this model glycoside hydrolase along its reaction pathway.

EXPERIMENTAL PROCEDURES

Protein Preparation. The expression and purification of full-length wild-type and mutant (H80A or H205A) Cex in *Escherichia coli*, and the subsequent isolation of the catalytic domain after proteolytic cleavage of the linker, were performed as described previously (*12*). The mutations were introduced using the QuikChange method (Stratagene). Unlabeled CexCD was obtained from bacteria grown in LB medium, whereas ^{15}N-labeled wild-type and mutant CexCD were prepared using M9 medium containing 1.0 g/L $^{15}NH_4$-Cl and 1.0 g/L [^{15}N]Celtone (Stable Spectral Isotopes, Inc.). CexCD, selectively labeled with [$^{13}C^{\epsilon 1}$]His, was expressed in a synthetic medium enriched with 75 mg/L ($^{13}C^{\epsilon 1}$, 99%) L-histidine·HCl·H_2O (Cambridge Isotope Laboratories, Inc.) (*13*). After protein purification, the buffer was exchanged by dialysis with 20 mM potassium phosphate (pH 6.5) and 0.02% NaN_3 for subsequent NMR spectroscopic analyses. Covalently inhibited 2FCb-CexCD was generated by addition of an ~3-fold molar excess of 2″,4″-dinitrophenyl 2-deoxy-2-fluoro-β-cellobioside to the purified protein. This complex is stable with a half-life of many months (*8*, *12*). Noncovalent complexes of CexCD were formed in the presence of an ~2-fold molar excess of xylobio-isofagomine [1,5-imino-1,4,5-trideoxy-3-*O*-(β-D-xylopyranosyl)-D-*threo*-pentitol] or xylobio-imidazole [(6*S*,7*S*,8*S*)-7,8-dihydroxy-6-(β-D-xylopyranosyloxy)-5,6,7,8-tetrahydroimidazole[1,2-α]pyridine] (*11*).

NMR Spectroscopy. Unless stated otherwise, all NMR spectra were recorded at 30 °C using a 600 MHz Varian INOVA spectrometer equipped with a gradient triple-resonance probe. NMR data were processed using NMRpipe (*14*) and analyzed using SPARKY (*15*). ^{1}H and ^{13}C chemical shifts were referenced to an external sample of DSS (sodium 2,2-dimethyl-2-silapentane-5-sulfonate) and ^{15}N shifts referenced indirectly via chemical shift ratios (*16*). Experiments used for this study included gradient versions of a one-dimensional (1D) jump-and-return echo (*17*), two-dimensional (2D) jump-and-return echo NOESY (*17*), one-bond sensitivity-enhanced ^{15}N HSQC (*18*), non-sensitivity-enhanced ^{15}N HSQC with a total INEPT delay of 22 ms to select for multiple-bond correlations while suppressing direct couplings (*19*), one-bond constant-time ^{13}C HSQC (*20*), one-bond sensitivity-enhanced ^{13}C HSQC with a CPMG pulse train (*21*), and a CβHδ (*22*, *23*). $^1J_{NH}$ couplings were measured from ^{15}N IPAP-HSQC spectra (*24*), as well as 1D jump-and-return echo and 2D ^{15}N HSQC spectra recorded without ^{15}N decoupling during the observation period.

Hydrogen Exchange. Proton−deuterium exchange (HX) measurements were carried out by passing unlabeled CexCD and 2FCb-CexCD through a 2.5 mL Sephadex G-25 medium spin column in a table top centrifuge to rapidly transfer the protein into 99% D_2O buffer containing 20 mM sodium phosphate and 0.02% NaN_3 (pH* 6.5) (*25*). A time series of ^{1}H NMR spectra were recorded at 20 °C starting ~5 min after transfer. Magnetization transfer-based proton−proton exchange measurements were recorded with 2FCb-CexCD at 10 °C using the CLEANEX-PM pulse sequence (*26*). Rate constants were determined using a MatLab macro provided by W.-Y. Choy (University of Toronto, Toronto, ON).

pK_a Measurements. Histidine pK_a values were determined from the pH dependence of the imidazole $^1H^{\epsilon 1}$ and $^{13}C^{\epsilon 1}$ chemical shifts of CexCD and 2FCb-CexCD selectively labeled with [$^{13}C^{\epsilon 1}$]His. The chemical shifts were measured using ^{13}C-CPMG-HSQC spectra (*21*), each recorded in 10−30 min. The pH of the protein samples was first increased and then decreased in 0.2−0.3 unit increments from a starting value of 6.5 by the addition of microliter aliquots of 0.1−0.5 M NaOH and HCl, respectively. The pK_a values were obtained by fitting the measured chemical shifts as a function of pH to the standard equations describing one or two macroscopic protonation equilibria (*27*). In the case of biphasic titration curves, the histidine pK_a was taken from the major, co-incident $^1H^{\epsilon 1}$ and $^{13}C^{\epsilon 1}$ chemical shift changes, with any minor changes attributed to the ionization of neighboring residues in the protein. Errors are estimated to be ±0.1 unit for all pH measurements and fit pK_a values.

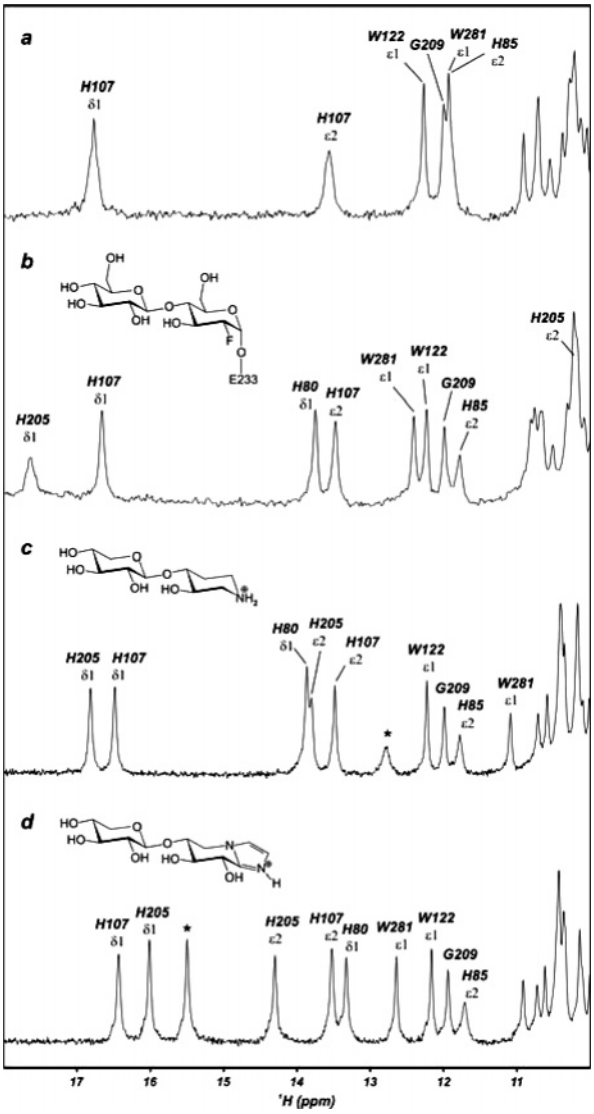

FIGURE 1: Jump-and-return echo ^{1}H-NMR spectra of the downfield region of (a) apo-CexCD, (b) covalently inhibited 2FCb-CexCD, and CexCD noncovalently inhibited with (c) xylobio-isofagomine and (d) xylobio-imidazole, at pH 6.5 and 30 °C. The assigned histidine signals arise from labile nitrogen-bonded imidazole protons that are protected from HX. Downfield peaks in panels c and d denoted with an asterisk are attributed to the bound inhibitors, with the xylobio-imidazole in its cationic form and the xylobio-isofagomine either neutral or positively charged (as assumed for the drawn structure). The amide $^1H^N$ resonance of Gly209 is likely shifted downfield due to a strong hydrogen bond to the side chain carboxyl of Asp253. The downfield indole $^1H^{\epsilon 1}$ resonances of Trp122 and Trp281 are attributed to hydrogen bonding to a buried water and to the side chain carboxyl of Asp235, respectively (*12*).

Enzyme Kinetics. The pH dependence of k_{cat}/K_m for full-length H80A Cex was determined at 37 °C in 150 mM NaCl and 0.1% (w/v) bovine serum albumin (BSA), according to published methods (*8*, *28*). The synthetic substrate *p*-nitrophenyl β-xylobioside (*p*NP-Xb) was described previously (*4*).

RESULTS

Histidine NMR Assignments. A striking feature of the ^{1}H-NMR spectrum of CexCD is the presence of peaks with resonances downfield of ~11 ppm (Figure 1). Upon formation of a long-lived covalent glycosyl intermediate with 2FCb, the chemical shifts of several of these peaks are

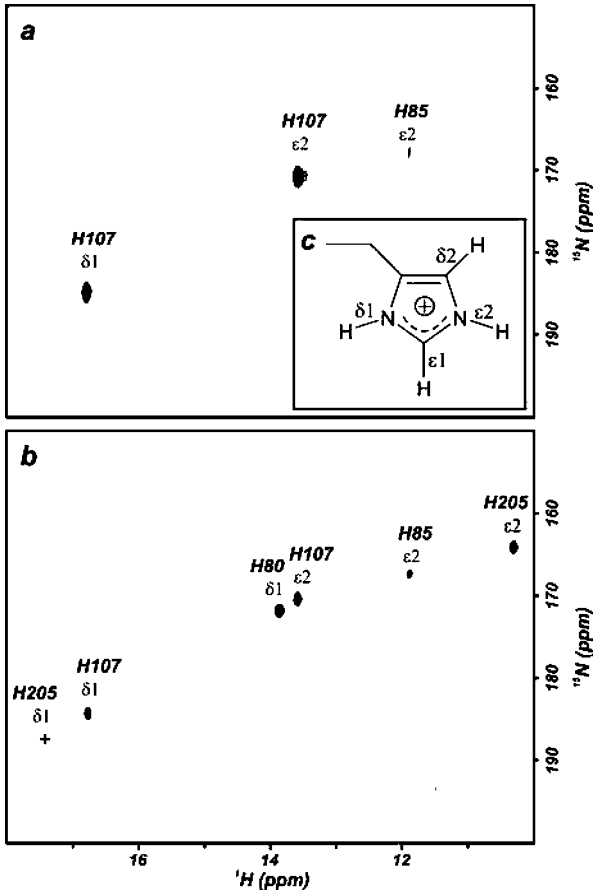

FIGURE 2: Assigned one-bond ^{15}N-HSQC spectra of ^{15}N-labeled (a) apo-CexCD and (b) covalently inhibited 2FCb-CexCD at pH 6.5 and 30 °C showing signals from protected imidazole ^{15}N−^{1}H pairs. The weak peak from the His205 $^{15}N^{\delta 1}-1H^{\delta 1}$ (indicated by a +) is not seen at this contour level. Panel c summarizes the nomenclature of the imidazole ring.

perturbed and three additional downfield signals are observed. With ^{15}N-labeled protein samples, each of these peaks exhibits a splitting of ~85−100 Hz due to a one-bond ^{1}H−^{15}N coupling and thus must arise from nitrogen-bonded imidazole, indole, or amide protons. In ^{15}N-HSQC spectra, three of these ^{1}H signals in apo-CexCD and six in 2FCb-CexCD show one-bond correlations to ^{15}N nuclei with chemical shifts in the range of 160−190 ppm (Figure 2), indicative of a protonated imidazole nitrogen (*29*). In general, the labile histidine $^1H^{\delta 1}$ and $^1H^{\epsilon 2}$ are observed only if protected from HX due to hydrogen bonding and/or burial within the interior of a protein.

The downfield region of the ^{1}H-NMR spectrum of CexCD also changes significantly with the noncovalent binding of xylobio-isofagomine [K_i = 0.13 μM at pH 7 (*11*)] and xylobio-imidazole (K_i = 0.15 μM) (Figure 1). In addition to six histidine signals, confirmed from ^{15}N-HSQC spectra of the ^{15}N-labeled protein (not shown), one extra peak is observed with each inhibitor arising from a ^{1}H not directly bonded to ^{15}N. These are tentatively assigned to the protected ^{14}N-bonded protons from the unlabeled xylobio-imidazole in its cationic form and the xylobio-isofagomine in either its charged or neutral form (*30*). In principle, such signals could arise from a buried phenolic or carboxylic proton in the protein or, much less likely on the basis of their chemical shifts, from a hydroxyl proton in either the protein or bound inhibitor. However, this seems unlikely since similar signals

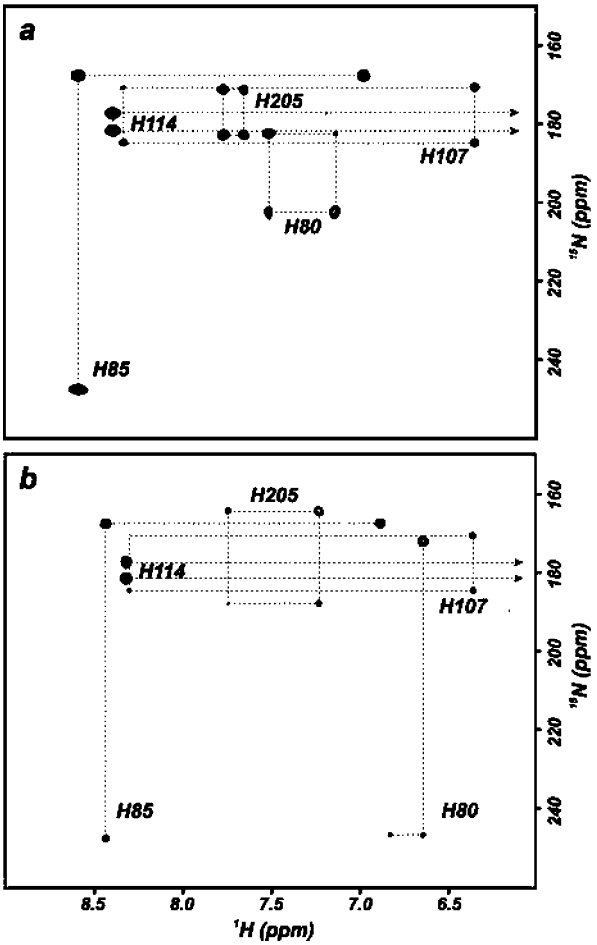

FIGURE 3: Assignment of the protonation and tautomerization states of the five histidine residues in ^{15}N-labeled (a) CexCD and (b) covalently inhibited 2FCb-CexCD at pH 6.5 and 30 °C from multiple-bond ^{15}N-HSQC spectra. Cross-peaks arise due to $^{2}J_{NH}$ and $^{3}J_{NH}$ couplings between $^{15}N^{\delta1}$ and $^{15}N^{\epsilon2}$ and carbon-bonded $^{1}H^{\delta2}$ and $^{1}H^{\epsilon1}$ nuclei within the imidazole rings (*29*). The upfield-shifted peaks involving the $^{1}H^{\delta2}$ of His114 at 3.79 ppm are not shown.

are not observed with 2FCb-CexCD. Unambiguous assignments could be obtained through the laborious synthesis of these inhibitors in ^{15}N- or ^{13}C-labeled forms.

The ^{1}H, ^{13}C, and ^{15}N resonances from the five imidazole rings in apo-CexCD and inhibited CexCD were assigned by three general approaches. First, from TROSY-based ^{1}H, ^{13}C, ^{15}N correlation experiments, the signals from the main chain nuclei in a ^{2}H-, ^{13}C-, and ^{15}N-labeled sample of the protein were assigned (*12*). Using these data, the CβHδ spectrum provided a correlation from the $^{13}C^{\beta}$ to the ring $^{1}H^{\delta2}$, which was then connected to the $^{13}C^{\delta2}$ in a constant-time ^{13}C-HSQC spectrum of the triply labeled protein. The nonlabile $^{1}H^{\delta2}$ and $^{1}H^{\epsilon1}$ were correlated to one another and to the neighboring $^{15}N^{\delta1}$ and $^{15}N^{\epsilon2}$ by multiple-bond ^{15}N-HSQC spectra of ^{15}N-labeled proteins (Figure 3). Parenthetically, HSQC experiments with an INEPT delay of 22 ms to select for two- and three-bond ^{1}H$-^{15}$N correlations while suppressing one-bond correlations gave better spectra than the standard non-refocused HMBC counterpart (*31*). This reflects the use of gradients, reduced perturbation of water magnetization, and the ability to phase the final spectra in pure absorption mode. A non-sensitivity-enhanced HSQC sequence was used to avoid excessive relaxation during the reverse INEPT transfer. The multiple-bond experiment also defined the charge states and tautomeric forms of the imidazole rings (*29*). These conclusions were corroborated by considering the corresponding $^{13}C^{\delta2}$ chemical shift of each residue (*32*). The $^{1}H^{\epsilon1}$ were then connected to the directly bonded $^{13}C^{\epsilon1}$ in a constant-time ^{13}C-HSQC spectrum of the uniformly ^{13}C-labeled protein, as well as in a ^{13}C-CPMG-HSQC spectrum of CexCD selectively labeled with [$^{13}C^{\epsilon1}$]His (Figure 4). The CPMG pulse train in this latter experiment led to a small increase in the signal-to-noise ratio, particularly with His80, likely due to refocusing of conformational exchange broadening. For protected $N^{\delta1}H$ and $N^{\epsilon2}H$, assignments of protonated nitrogens were determined from a one-bond ^{15}N-HSQC spectrum (Figure 2). A second parallel approach was undertaken using ^{1}H$-^{1}$H NOESY spectra to assign signals from the protected $^{1}H^{\delta1}$ and $^{1}H^{\epsilon2}$ on the basis of intra- and interresidue interactions with neighboring protons in the two forms of the protein. Finally, to confirm these assignments, spectra were also recorded with apo and inhibited forms of CexCD containing alanine substitutions at His80 or His205 (not shown). These assignments, summarized in Table S1 of the Supporting Information, have been deposited in the BioMagResBank as accession numbers 7264 and 7265.

Histidine HX. The observation of ^{15}N-HSQC signals from the labile nitrogen-bonded protons of His85 and His107 in CexCD, plus those of His80 and His205 in the inhibited species (Figures 1 and 2), indicates that these protons are protected from rapid HX. However, none of these signals were observed in 1D spectra of apo- and 2FCb-CexCD recorded immediately after either form of the protein was transferred into D_2O buffer (pH* 6.5 and 20 °C), demonstrating that their exchange lifetimes are all less than the ~5 min dead time of this approach. Accordingly, the CLEANEX-PM experiment (*26*) was used to measure rapid proton$-$proton HX. Detectable exchange in 2FCb-CexCD was observed for only H85 $^{1}H^{\epsilon2}$ and H205 $^{1}H^{\epsilon2}$, with pseudo-first-order rate constants of 16.5 $\pm$ 1 and 12.5 $\pm$ 0.7 s^{-1}, respectively (pH 6.5 and 10 °C). Thus, the lifetimes for the remaining labile imidazole protons, observed in the ^{15}N-HSQC spectra of apo- and 2FCb-CexCD, must fall between the limits of these two experimental approaches (i.e., from 0.1 to 300 s). These limits correspond to HX ~$10^{2}-10^{5}$-fold slower than that expected for a nitrogen-bonded proton in a free imidazole under similar conditions [~1 ms (*25*)]. By way of comparison, the highly protected $^{1}H^{\epsilon2}$ of a buried neutral histidine in *Bacillus circulans* xylanase exchanges with a lifetime of ~7 h at 30 °C and pH* 7 (*33*), whereas the detectable $^{1}H^{\delta1}$ of His57 in a rat trypsin mutant exchanges with lifetimes of 2$-$12.5 ms in its apo and two inhibited forms at 5 °C and pH 5.2 or 10 (*34*).

Histidine pK_a Values. The pK_a values (or limits thereto) of the five histidines in apo- and 2FCb-CexCD were determined from the pH dependence of their $^{13}C^{\epsilon1}$ and $^{1}H^{\epsilon1}$ shifts (Figure 5 and Table 1). These measurements were carried out using selectively [$^{13}C^{\epsilon1}$]His-labeled protein, for which well-resolved ^{13}C-HSQC spectra could be obtained within minutes (Figure 4). This approach (*35*, *36*) is significantly more sensitive than direct ^{15}N detection (*33*, *37*) or indirect two- or three-bond $^{1}H^{\delta2/\epsilon1}-^{15}N^{\delta1/\epsilon2}$ correlation experiments (*19*). Although not needed with the 34 kDa CexCD, background deuteration should facilitate the applicability of this approach to higher molecular mass systems.

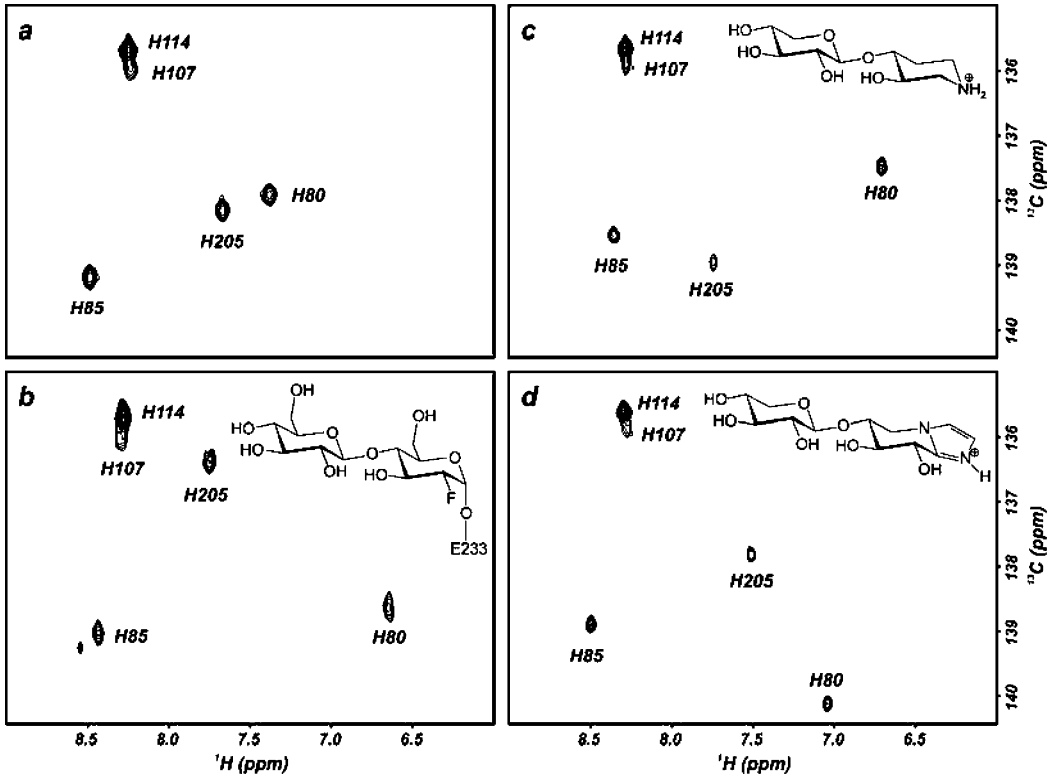

FIGURE 4: Assigned one-bond ^{13}C-CPMG-HSQC spectra of selectively [$^{13}C^{\epsilon 1}$]His-labeled (a) apo-CexCD, (b) covalently inhibited 2FCb-CexCD, and CexCD noncovalently inhibited with (c) xylobio-isofagomine (assumed positive) and (d) xylobio-imidazole, at pH 6.5 and 30 °C.

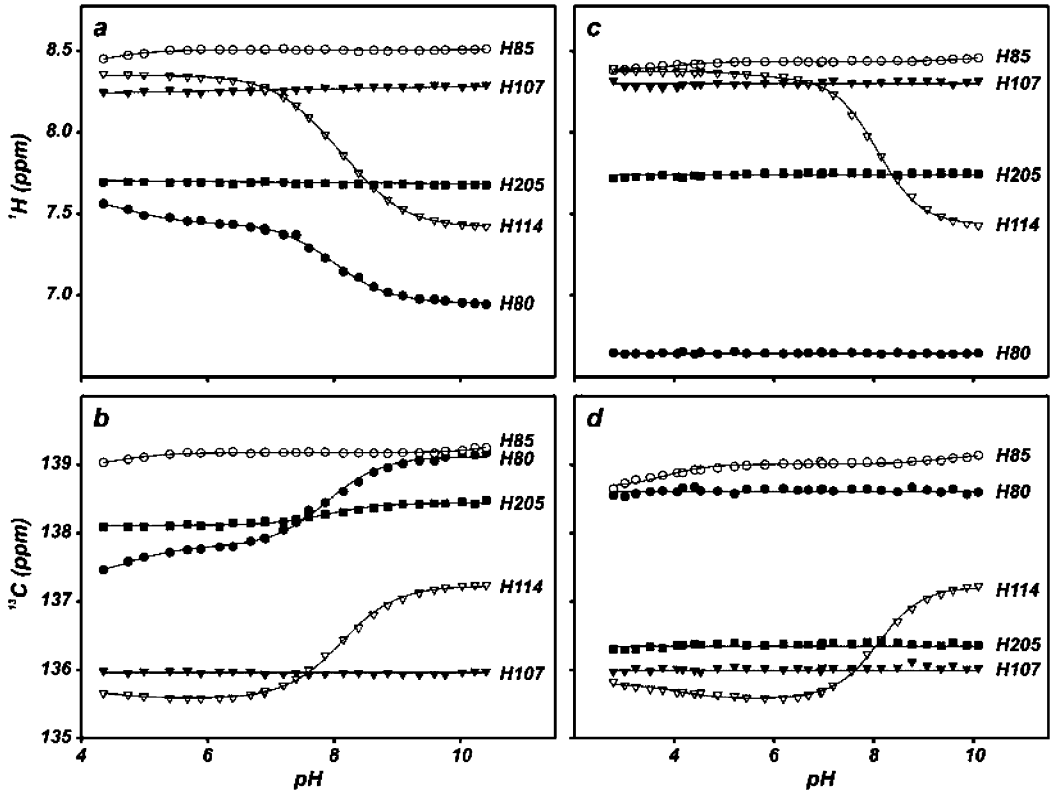

FIGURE 5: Determination of the pK_a values of the five histidines in (a and b) apoCexCD and (c and d) covalently inhibited 2FCb-CexCD at 30 °C from their pH-dependent (a and c) $^{1}H^{\epsilon 1}$ and (b and d) $^{13}C^{\epsilon 1}$ chemical shifts. The lines represent best fits to equations describing one, and when necessary, two macroscopic protonation equilibria.

Over a pH range of 4.3−10.5 for apo-CexCD, only His114 (pK_a = 8.1) and His80 (pK_a = 7.9) exhibited measurable titrations. Similarly for 2FCb-CexCD, over a pH range of 2.8−10.1, only His114 (pK_a = 8.1) titrated. Thus, the remaining histidines, with pH-independent chemical shifts, have pK_a values that are at least 1 unit outside these ranges (i.e., given that clear spectral changes should be seen at a pH of pK_a ± 1). However, on the basis of $^{13}C^{\epsilon 1}$ and $^{1}H^{\epsilon 1}$

Table 1: CexCD Histidine pK_a Values and Related Properties

residue	form	sequence conservation[a] (%)	accessible surface area[b] (Å^2)	structural features[c]	HX protected[d]	charge and tautomer at pH 6.5	pK_a[e]
His80	apo	100	2.7/0.0/2.1	$N^{\delta1}$ H-bond donor to buried D123 (2.9 Å)		titrating	7.9
	2FCb		0.8/0.0/0.0	$N^{\epsilon2}$ H-bond acceptor from inhibitor 3-OH group (2.7 Å)	$H^{\delta1}$	neutral $N^{\delta1}$	<2.8
His85	apo	71	22.9/0.2/11.8	3.4 Å to E127; 3.5 Å to R136;[f] $N^{\delta1}$ H-bond acceptor from buried water (3.0 Å)	$H^{\epsilon2}$	neutral $N^{\epsilon2}$	<4.0
	2FCb		26.5/0.3/14.6		$H^{\epsilon2}$	neutral $N^{\epsilon2}$	<2.8
His107	apo	60	0.0/0.0 /0.0	$N^{\delta1}$ H-bond donor to buried E52 (2.7 Å); $N^{\epsilon2}$ H-bond donor to buried water (2.8 Å)	$H^{\delta1}$, $H^{\epsilon2}$	positive	>10.4
	2FCb		0.0/0.0/0.0		$H^{\delta1}$, $H^{\epsilon2}$	positive	>10.1
His114	apo	28	47.6/19.7/0.0	$N^{\delta1}$ H-bond donor to surface water (2.8 Å); $N^{\epsilon2}$ H-bond donor to D64 (2.7 Å)		positive	8.1
	2FCb		48.2/20.7/0.0			positive	8.1
His205	apo	99	6.4/0.0/3.5	$N^{\delta1}$ H-bond donor to D235 (2.9 Å); $N^{\epsilon2}$ H-bond donor to E233 (2.9 Å)		positive	>10.4
	2FCb		6.2/0.0/0.0	$N^{\epsilon2}$ H-bond donor to inhibitor O5 (3.0 Å)	$H^{\delta1}$, $H^{\epsilon2}$	positive	>10.1

[a] Sequence conservation (identity) based on the alignment of 92 family 10 glycoside hydrolases from the SMART database (http://smart.embl-heidelberg.de/). [b] Calculated with MolMol (*70*) for each imidazole ring (ring/$H^{\delta1}$/$H^{\epsilon2}$) using a probe radius of 1.4 Å. [c] From PDB entry 2EXO for apo-CexCD and PDB entry 1EXP for 2FCb-CexCD. Structural features are given for only 2FCb-CexCD if they differ from the apoprotein. [d] Observable in a 1D jump-and-return or 2D ^{15}N-HSQC spectrum. [e] pK_a limits are set by the range of pH conditions utilized for a given titration. Actual pK_a values are likely at least 1 unit beyond these limits. Errors are ±0.1. [f] See Discussion for further clarification.

shifts alone, one cannot unambiguously establish if a histidine is neutral or charged within these pH limits. For example, although the $^{13}C^{\epsilon1}$ and $^{1}H^{\epsilon1}$ shifts of a neutral histidine in an unstructured polypeptide are downfield and upfield, respectively, relative to its charged form (*38*, *39*), in CexCD, neutral (see below) His85 has a $^{1}H^{\epsilon1}$ shift diagnostic of a charged group whereas protonated His205 has a $^{13}C^{\epsilon1}$ shift indicative of a neutral imidazole. These discrepancies reflect the additional local environmental effects on the NMR signals of each particular histidine.

Due to the extreme difference between the chemical shifts of a protonated and unprotonated imidazole nitrogen (*1*, *29*, *37*, *40*), the charge states of the histidines in apo- and 2FCb-CexCD can be determined unambiguously by consideration of their ^{15}N assignments obtained at pH 6.5 (Figure 3). Thus, in apo- and 2FCb-CexCD, the nontitrating His85 is neutral and, on the basis of the observed pattern of $^{2}J_{NH}$ and $^{3}J_{NH}$ couplings, in the common $N^{\epsilon2}$ tautomeric state. By contrast, His107 and His205 are both positively charged. Upon formation of 2FCb-CexCD, His80 adopts the $N^{\delta1}$ tautomeric form at neutral pH, with its pK_a dropping from 7.9 to a value below the measured limit of 2.8.

The pK_a values of the histidines in the complexes of CexCD with xylobio-imidazole and -isofagomine were not measured. However, at pH 6.5, their ionization states in both complexes are likely similar to that of 2FCb-CexCD, which is evident from multiple-bond ^{15}N-HSQC spectra (not shown). Thus, the pK_a of His80 appears to drop from 7.9 to values significantly below 6.5 upon noncovalent inhibition with the two xylobiose derivatives.

DISCUSSION

Using a combination of ^{1}H, ^{13}C, and ^{15}N chemical shift information and qualitative two- and three-bond $^{1}H-^{15}N$ correlation measurements, we obtained a comprehensive description of the pH dependence of the ionization and tautomerization behavior of the five histidines in CexCD. In summary, for the apoenzyme at its pH optimum of ~6, His107 and His205 are positively charged, His85 exists as the neutral $N^{\epsilon2}$ tautomer, and His114 and His80 are titrating between predominantly positively charged imidazolium ion and neutral imidazole states. Upon formation of two noncovalent enzyme−inhibitor complexes or a long-lived covalent glycosyl−enzyme intermediate, the chemical shifts of His80 and His205, which are located within the active site of the enzyme, are markedly perturbed. Furthermore, the labile protons from these two histidines become protected from exchange with water, with His80 adopting a neutral $N^{\delta1}$ tautomeric state and His205 remaining positively charged. These results, summarized in Table 1, can be interpreted for each histidine by considering the high-resolution crystal structures of apo- and 2FCb-CexCD (PDB entries 2EXO and 1EXP, respectively; Figure 6), as well as those of the inhibited H127A/H205A-CexCD mutant (PDB entry 2HIS) and XbIso·CexCD (PDB entry 1FH8) and XbIm·CexCD (PDB entry 1FDH), combined with electrostatic calculations presented in Table S2 of the Supporting Information.

Non-Active Site Histidines

His107. Located within the interior of CexCD, the nitrogen-bonded protons of the moderately conserved His107 are well protected from HX through hydrogen bonding with Glu52 and an internal water. Although fully buried, the formation of a strong salt bridge with this presumably charged glutamate increases the pK_a of His107 to >10.4.

His114. Nonconserved His114 lies on the surface of CexCD, donating hydrogen bonds to a crystallographically bound water and to the carboxyl of nearby Asp64. These interactions, which do not lead to measurable HX protection, help increase the pK_a value of His114 to 8.1. Unlike the previous case of the buried His107-Glu52 charge pair within the low-dielectric interior of CexCD, the pK_a value of the solvent-exposed His114 is only ~1.5 units higher than that expected for a histidine in a random-coil polypeptide. As noted previously, the least conserved electrostatic interactions

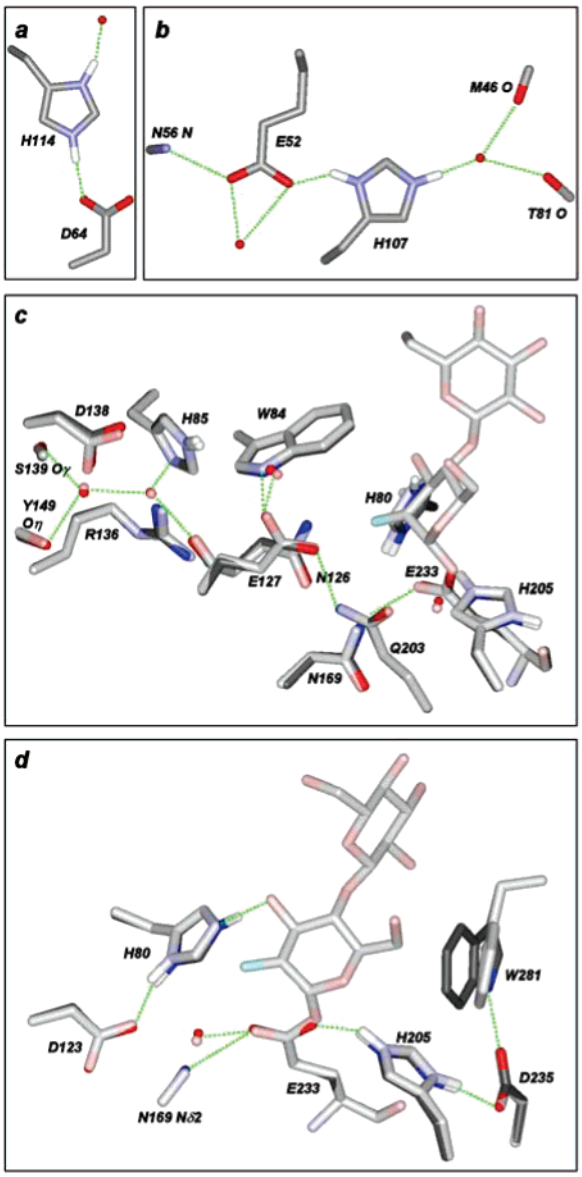

FIGURE 6: Salient features of the structural environments of (a) His114, (b) His107, and (c and d) His80, His85, and His205 in CexCD (blue for nitrogen, red for oxygen, gray for carbon; only imidazole hydrogens (white) are shown). Also presented in panels c and d, which differ by a rotation of ~90° about the vertical axis, is the superimposed structure of covalently inhibited 2FCb-CexCD (light coloring; cyan for fluorine). This figure was generated using the crystallographic coordinates of PDB entry 2EXO for CexCD and PDB entry 1EXP for 2FCb-CexCD.

in a family of related proteins generally occur with surface residues and are associated with relatively unperturbed pK_a values (*41*, *42*). Interestingly, the imidazole of His114 stacks against a corner formed by the orthogonal rings of Phe60 and Phe115. Shielding due to the net ring currents from these aromatic groups alters the $^1H^{\delta 2}$ chemical shift of this histidine to a highly anomalous value of 3.79 ppm.

Active Site Histidines

His80. In apo-CexCD, the completely conserved and slightly exposed His80 lies within the active site cleft of the protein, donating its $H^{\delta 1}$ in a hydrogen bond to buried Asp123. Along with electrostatic effects (~4 Å) from the nucleophile Glu233 and Lys47, this interaction helps to increase the pK_a value of His80 to 7.9 but does not significantly protect its labile imidazole protons from HX. Remarkably, upon formation of the covalent glycosyl−enzyme intermediate with 2FCb, the pK_a of this residue drops by more than 5 units to <2.8 and its $^1H^{\epsilon 2}$ can now be observed in a ^{1}H-NMR spectrum. Although not determined quantitatively, the pK_a of His80 also decreases in the presence of the xylobio-isofagomine and -imidazole inhibitors. In each of these three cases, the neutral His80 adopts the less common $N^{\delta 1}H$ tautomer and thereby continues donating a hydrogen bond to Asp123, while accepting one via its unprotonated $N^{\epsilon 2}$ from the exocyclic 3-OH of the bound sugar. Previously, either the ionized form or the opposite tautomer of this histidine has been assumed in X-ray crystallographic analyses of inhibited Cex and related family 10 glycosyl hydrolases such that both His80 and Lys47 would be donating hydrogen bonds to the 3-O of the substrate (*5*, *10*, *30*, *43*). Burial of His80 by the inhibitor and/or possible changes in the dynamic properties of the surrounding active site region of Cex (*12*) likely lead to an increased level of protection of the labile $H^{\delta 1}$ from rapid solvent exchange.

The reduced pK_a of His80 in 2FCb-CexCD may be a necessary consequence of the hydrogen bonding arrangement observed at that location. That is, upon covalent linkage to CexCD, the 3-OH group of the bound substrate becomes completely buried within the active site of the enzyme. Since the oxygen is accepting a hydrogen bond from Lys47, which is unambiguously in its $-NH_3^+$ form with a pK_a of >9 (*44*), it must be donating a hydrogen bond to His80. For the lone pair of electrons on the imidazole $N^{\epsilon 2}$ of His80 to accept this hydrogen bond, the imidazole cannot also remain protonated at that position. The neutralization of nearby Glu233 due to its covalent linkage to the bound inhibitor and/or possible changes in local dielectric due to solvent exclusion may also disfavor His80 remaining postively charged in 2FCb-CexCD. In the cases of the xylobiose-derived inhibitors, repulsion from the potentially ionized isofagomine or imidazole groups (*30*, *43*) may contribute further to the reduced pK_a value of His80. Interestingly, in apo-CexCD, the $^1H^{\epsilon 1}$ and $^{13}C^{\epsilon 1}$ of His80 also exhibit small chemical shift changes corresponding to a titration with an apparent pK_a of ~4.7 (Figure 5). This may reflect the deprotonation of Asp123 to which His80 is hydrogen bonded, thereby forming a buried ion pair. Furthermore, such chemical shift changes are not seen with 2FCb-CexCD, suggesting that the pK_a of Asp123 also changes along with that of His80. If so, this might imply a maintenance of net charge neutrality in this region of Cex by the formal transfer of the imidazolium proton of His80 to the carboxylate of Asp123 upon formation of the glycosyl−enzyme intermediate. We are currently attempting to address this hypothesis by directly measuring the pK_a values of the Asp and Glu residues in CexCD. However, detecting and assigning the pH-dependent $^{13}C^{\gamma}$ and $^{3}C^{\delta}$ signals, respectively, from the large number of carboxyl side chains in this 34 kDa protein is a challenging task.

By thermodynamic linkage, the decrease in the pK_a value of His80 upon inhibitor binding necessitates that the contribution by His80 toward substrate binding will be favored with an increase in pH. Thus, *solely* on the basis of its pK_a values, at the pH optimum of CexCD (~6), the deprotonation of His80 upon formation of the glycosyl−enzyme intermedi-

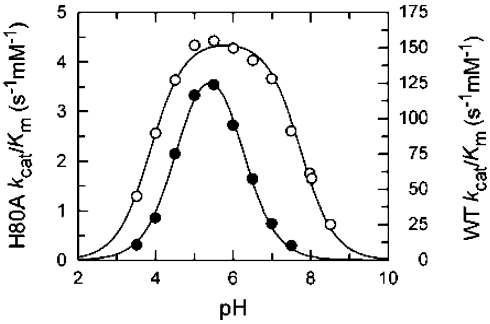

FIGURE 7: Mutation of His80 to alanine changes the pH dependence of k_{cat}/K_m. The activity profile of full-length H80A Cex toward *p*NP-Xb (●) is fit to a bell-shaped curve with apparent pK_a values of 4.6 and 6.6. The activity of WT Cex toward *p*NP-Cb (○) follows pK_a values of 4.1 and 7.7 (reproduced from ref *8*). Note that, with WT Cex, k_{cat}/K_m is ~100-fold higher toward *p*NP-Xb vs *p*NP-Cb (*4*). Also, the pH dependence of k_{cat}/K_m reflects ionization events within the free enzyme and thus should not differ between the two closely related neutral substrates.

ate leads to a free energy penalty of ~2.8 kcal/mol (*45*). This linkage should be manifest in a pH dependence of the kinetic parameters of Cex for its substrates or of the K_i values for its inhibitors. However, interpreting such effects is difficult due to the complex network of additional ionizable groups (also with changing pK_a values upon substrate binding) in the active site of this enzyme, including Asp123 and Glu233. Also, the K_m value of Cex is dependent upon the kinetic parameters governing both the glycosylation and deglycosylation steps in its double-displacement mechanism.

The catalytic importance of His80 is confirmed by an ~2000-fold decrease in k_{cat}/K_m from 1500 mM^{-1} s^{-1} for wild-type Cex to 0.72 mM^{-1} s^{-1} for the H80A mutant toward the synthetic substrate pNP-Xb (pH 7 and 37 °C) (*46*). Furthermore, as shown in Figure 7, the pH dependence of k_{cat}/K_m differs significantly between the two species. In its simplest interpretation, the bell-shaped activity profile of wild-type Cex indicates that a group with an apparent acidic limb pK_a value of ~4.1 in the *free* enzyme must be deprotonated for catalysis to occur, whereas another with an apparent basic limb pK_a value of ~7.7 must remain protonated (*8*, *9*). These groups can be assigned tentatively to the nucleophile, Glu233, and the general acid, Glu127, respectively. However, site-specific pK_a measurements for the two catalytic side chains, as well as for all other ionizable active site residues (which may exhibit coupled microscopic protonation equilibia with Glu127 and Glu233), are required to confirm this conclusion (*47*). In particular, the observation that the NMR-determined pK_a of 7.9 for His80 is similar to the basic limb value of ~7.7 raises the interesting possibility that the ionization of this histidine contributes to a kinetic pK_a governing the pH-dependent activity profile of CexCD. In contrast to the WT enzyme, the k_{cat}/K_m profile of the H80A mutant follows apparent pK_a values of 4.6 and 6.2. The acid limb shift toward a higher pH implies that the apparent pK_a value of Glu233 increased upon removal of a favorable electrostatic interaction with the nearby His80 ($N^{\epsilon 2}-O^{\gamma}$ separation of ~4 Å). However, the concomitant decrease in the basic limb pK_a value is the opposite of that expected for loss of a favorable interaction with Glu127 ($N^{\epsilon 2}-O^{\gamma}$ separation of ~7 Å). Thus, additional structural and electrostatic changes within the tightly coupled active site of Cex must accompany the mutation of His80. Although difficult to interpret, these kinetic measurements nevertheless demonstrate that His80 plays a key role in establishing the pH-dependent activity of Cex.

His85. The moderately conserved His85 lies partly buried near the surface of the active site of the protein and in the proximity to the guanidinium group of Arg136, as well as the carboxyl of the general acid/base catalyst Glu127. His85 has a pK_a value of <2.8 and remains in neutral $N^{\epsilon 2}H$ tautomeric form under all pH conditions that were examined. It is somewhat surprising that the labile $H^{\epsilon 2}$ is sufficiently protected from HX to be detected by ^{1}H-NMR, as within the available crystal structures of CexCD, it is exposed to the solvent. Flipping the imidazole ring of His85 about its $C^{\beta}-C^{\gamma}$ bond would decrease the accessible surface area of the $N^{\epsilon 2}H$ group, while also allowing a very weak hydrogen bond (~3.3 Å) to the side chain of Glu127. However, this would leave a buried water with an unsatisfied hydrogen bond to a site currently identified in the crystallographically determined structures as $N^{\delta 1}$ of His85. The 2D jump-and-return echo NOESY spectrum does not help resolve this discrepancy since no inter-residue NOEs were observed to the $H^{\epsilon 2}$ of His85. The low pK_a value of this histidine, which likely results from Arg136 charge repulsion, is also not fully expected given that Glu127, as well as Asp138, are adjacent to its imidazole ring. However, by analogy to the well-studied example of *B. circulans* xylanase (*47*), it is anticipated that in apo-CexCD, Glu127 has a pK_a value [tentatively 7.7 by kinetic measurements as discussed above (*9*)] that is greater than the pH optimum of the enzyme so that it can serve as a general acid yet lower than this value in the glycosyl−enzyme intermediate where it functions as a general base. Thus, at least for apo-CexCD, Glu127 would be negatively charged only at elevated pH values, and any stabilization of His85 in a protonated state by this catalytic glutamate would be offset by the intrinsic pK_a of the histidine, which favors the neutral form under basic conditions. In the end, the net effect of these complex pH-dependent interactions is to dramatically decrease the pK_a of His85 in the apo and inhibited forms of CexCD.

Unfortunately, for unknown reasons, we were unable to produce Cex with the H85A substitution despite testing a variety of bacterial expression conditions. Also, we were unsuccessful at generating mutants of Cex encoding a glutamine or asparagine at this position. Thus, the contributions of His85 to the pH-dependent activity of Cex could not be investigated further through site-directed mutagenesis.

His205. In apo-CexCD, the highly conserved His205 bridges Asp235 and the nucleophile, Glu233. Surprisingly, although donating hydrogen bonds to both carboxylates, neither of its labile imidazole protons is protected significantly from HX. pH-dependent kinetic measurements suggest that Glu233 has an apparent pK_a value of ~4.1 in the free enzyme (*9*), whereas the charge state of buried Asp235 has not yet been determined. These two hydrogen bonding interactions must help increase the pK_a of His205 to >10.4 such that the histidine is positively charged under all conditions that have been examined. Upon formation of the glycosyl−enzyme intermediate, the pK_a value of His205 remains >10.1, despite the loss of a favorable electrostatic interaction with Glu233 (now neutral in a glycosidic linkage).

This may be compensated by formation of a bifurcated hydrogen bond from its $N^{\epsilon 2}H$ to both Glu233 (2.9 Å) and O5 of the proximal sugar ring (3.0 Å). In the cases of the xylobiose-derived inhibitors, His205 also remains positively charged, with its $N^{\epsilon 2}H$ strongly hydrogen bonded (~2.7 Å) to Glu233, while also in van der Waals contact with carbons in the isofagomine or imidazole rings. As discussed below, the ~3 ppm downfield shift of His205 $^1H^{\epsilon 2}$ in XbIso·CexCD and XbIm·CexCD relative to 2FCb-CexCD (Figure 1) likely results from differences in the ionization state of the hydrogen bond acceptor, Glu233. It is highly probable that the nucleophilic glutamate remains negatively charged in XbIso·CexCD and XbIm·CexCD, whereas it become neutral due to covalent modification in 2FCb-CexCD. As with His80, upon formation of either the noncovalent inhibitor complexes or the covalent glycosyl−enzyme intermediate, the labile imidazole protons of His205 become protected from exchange with water, due to solvent exclusion and/or a reduction in local active site dynamics (*12*).

Consistent with the intimate contact between His205 and the nucleophile Glu233, mutation of this histidine residue to an alanine or asparagine severely (~10^4-fold) decreases the k_{cat}/K_m value of Cex toward substrates such as *p*NP-Cb (*28*). As also discussed in a previous structural study of these mutants, substitution of His205 with a neutral side chain dramatically alters the pH-dependent activity profile of Cex such that no essential ionization is detected between pH ~4 and 9 (*28*). While not readily interpretable, this verifies the catalytic importance of His205.

Xylobiose-Derived Aza-Sugar Inhibitors

Signals tentatively assigned to nitrogen-bonded protons in xylobio-isofagomine and -imidazole were also detected when these inhibitors were complexed with CexCD at pH 6.5. These protons are likely protected from rapid HX due to hydrogen bonding with active site residues, including Glu127, Gln203, and Glu233. In a detailed crystallographic analysis of four aza-sugar inhibitors bound to CexCD at pH 4.6, each was inferred to have a positively charged nitrogen (*10*). This appears to hold true for the xylobio-imidazole since a proton assigned to its ring nitrogen is observed in the ^1H-NMR spectrum of XbIm·CexCD. Furthermore, this indicates that the pK_a of the bound xylobio-imidazole is likely elevated from its solution value of 5.9 (J. Wicki and S. G. Withers, unpublished observations) due to favorable active site electrostatic interactions. This conclusion is also consistent with the atomic-resolution X-ray crystallographic structure of cationic glucoimidazole bound to a family 5 endoglucanase at pH 5.5 (*48*), and as inferred from the pH-dependent inhibition of a family 1 β-glycosidase by glucoimidazole derivatives (*49*).

In contrast, the charge state of the xylobiose-isofagomine cannot be determined solely from the ^1H NMR spectrum of XbIso·CexCD. However, on the basis of a measured pK_a value of 8.8 in solution (J. Wicki and S. G. Withers, unpublished observations), this inhibitor should also be positively charged when bound to CexCD. If so, then both nitrogen-bonded protons of the isofagomine moiety likely have degenerate chemical shifts in the spectrum in Figure 1C. In a 1.05 Å resolution crystal structure of inhibited *Bacillus agaradhaerens* Cel5A at pH 5, cellobio-isofagomine was clearly protonated with electron density observed for two hydrogens bonded to its ring nitrogen (*43*). In an ~1 Å resolution structure of *Streptomyces lividans* Xyn10a, which is highly similar to Cex, the charge state of bound xylobiose-isofagomine remained ambiguous at both pH 5.8 and 7.5. However, the ligand nitrogen was inferred to be positively charged on the basis of the pH dependence of its inhibition constant, K_i (*30*). Kinetic inhibition and isothermal titration calorimetry studies also indicated that isofagomine binds preferentially to a family 1 β-glucosidase in its conjugate acid form (*50*). In principle, if synthesized in a ^{15}N-labeled form, the protonation state of the isofagomine group in XbIso·CexCD could be determined unambiguously from its pH-dependent ^{15}N chemical shifts and $^1J_{NH}$ coupling patterns (*44*), thereby providing further insights into the mechanism of CexCD inhibition.

Histidine pK_a Values and pK_a Calculations

The pK_a value of a histidine in a random coil polypeptide is typically ~6. In stark contrast, the pK_a values of the five histidine residues in CexCD vary from <2.8 to >10.4 and that of His80 drops from 7.9 to <2.8 upon formation of the glycosyl−enzyme intermediate. Abnormally low pK_a values (<3) have also been reported for histidine residues in proteins such as *B. circulans* xylanase (*33*), *B. agaradhaerens* xylanase (*51*), and subtilisin BPN′ (*52*), whereas elevated pK_a values of 9.1 and 10.4 have been measured for salt-bridged histidine side chains in T4 lysozyme (*45*) and superoxide dismutase (*53*), respectively (see also ref *42* and http://www.jenner.ac.uk/PPD/). Thus, the acid dissociation constant of a histidine can vary by at least 10^8-fold depending upon its structural and electrostatic environment within a protein and can dramatically change along the reaction pathway of a single enzyme.

The accurate calculation of pK_a values of ionizable groups in proteins remains a theoretical and practical challenge. A summary of predictions using WHAT IF (*54*) and PropKa (*55*) for the five histidines in CexCD is presented in Table S2 of the Supporting Information. After optimization of hydrogen bonding networks, WHAT IF calculates pK_a values by solving the linearized Poisson−Boltzmann equation to describe the electrostatic interactions within a protein, followed by a Monte Carlo analysis to define the lowest-energy ionization states as a function of pH (*54*). In contrast, PropKa rapidly predicts pK_a values for ligand-free protein residues using empirical rules for desolvation, hydrogen bonding, and Coulombic interactions (*55*). Relative to a random coil polypeptide reference state, PropKa correctly predicted the signs of the pK_a changes (i.e., positive or negative) for His85, His114, and His205 in apo-CexCD yet tended to underestimate their magnitudes. In the case of His80 and His107, the signs of the changes were also incorrect. These errors may result from an overestimation of the effects of desolvation to favor the neutral imidazole ring. In the case of apo-CexCD, WHAT IF correctly predicted the signs of the pK_a changes for all histidines yet both over- and underestimated their magnitudes by up to 2 log units. For 2FCb-CexCD, WHAT IF correctly predicted a decrease in the pK_a value of His80, attributable to an increased level of desolvation and neutralization of Glu233 upon formation of a glycosyl−enzyme intermediate yet

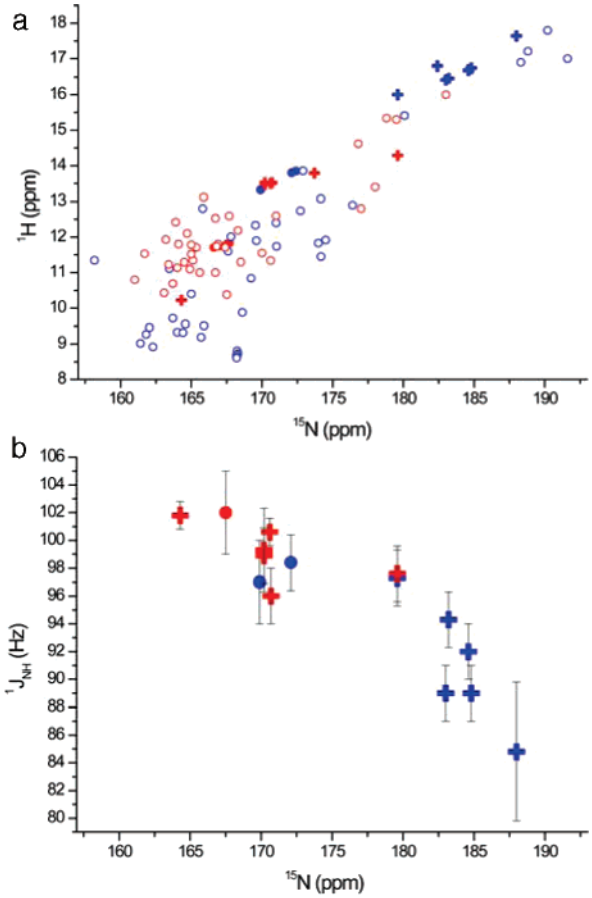

FIGURE 8: (a) Correlation of the $^1H^{\delta1}-^{15}N^{\delta1}$ (blue) and $^1H^{\epsilon2}-^{15}N^{\epsilon2}$ (red) chemical shifts for the histidines in apo-CexCD and inhibited CexCD (pH 6.5; filled circles, neutral; filled crosses, positively charged), as well as those reported in the literature and/or the BioMagResBank (empty circles, without specification of charge). (b) Correlation of $^1J_{HN}$ vs $^{15}N^{\delta1}$ (blue) and $^{15}N^{\epsilon2}$ (red) chemical shifts for the histidines in CexCD (filled circles, neutral; filled crosses, positively charged). On the basis of the relationship in panel a, a similar correlation is seen for $^1J_{HN}$ vs $^1H^{\delta1}$ and $^1H^{\epsilon2}$ chemical shifts (not shown).

significantly underestimated the magnitude of the change. Unexpectedly, the pK_a value of His205 was also predicted to drop dramatically due to a loss of stabilizing electrostatic interactions. These errors likely reflect the challenges in calculating the pK_a values of a system of highly coupled ionizable groups, as found in the active site of Cex. Nevertheless, both approaches provided valuable insights, discussed above, into the factors dictating the titration behaviors of the histidines in this enzyme. Conversely, the data from this study should facilitate the development of improved algorithms for protein electrostatic calculations.

Histidine Chemical Shifts

The chemical shifts of a histidine can also provide important insights into its structural and electrostatic environment within a protein. For example, using data measured herein for CexCD (Table S1 of the Supporting Information) and reported in the BioMagResBank, a striking linear relationship is found to exist between the ^{1}H and ^{15}N chemical shifts of directly bonded $^1H^{\delta1}-^{15}N^{\delta1}$ and $^1H^{\epsilon2}-^{15}N^{\epsilon2}$ histidine pairs (Figure 8A). Thus, both nuclei must be affected similarly by factors such as hydrogen bonding. In contrast, such a clear dependence is not seen for amide $^1H^N-^{15}$N pairs in proteins due to a complex interplay of sequence and structural effects. This simple relationship may help provide qualitative insights into the environments and charge states of histidine residues in proteins, for example, by allowing approximate chemical shift predictions for $^1H^{\delta1/\epsilon2}$ nuclei, which are not detected due to rapid HX, based on $^{15}N^{\delta1/\epsilon2}$ shifts measured from HMBC spectra. Further inspection of the data in Table S1 reveals that, within each fully protonated histidine in CexCD, the $^1H^{\delta1}$ and $^{15}N^{\delta1}$ nuclei have chemical shifts downfield from those of the corresponding $^1H^{\epsilon2}$ and $^{15}N^{\epsilon2}$ nuclei, respectively. This pattern, seen also for free histidine (*56*), however, does not hold for proteins in general (Figure 8A), thus precluding assignments based on shifts alone. Also, as noted previously (*1*), most positively charged histidines in CexCD have $^1H^{\delta1}-^{15}N^{\delta1}$ and $^1H^{\epsilon2}-^{15}N_\epsilon^2$ chemical shifts downfield of those from neutral histidines. However, His205 in 2FCb-CexCD stands as a noteworthy exception, with its $^1H^{\epsilon2}$ and $^{15}N^{\epsilon2}$ shifts rather upfield at 10.22 and 164.3 ppm, respectively. An explanation of this anomaly is provided by a comparison to the well-studied serine proteases.

His205 is hydrogen bonded to the nucleophile Glu233 and Asp235, forming a Asp235-His205-Glu233 constellation that is strikingly similar to the catalytic (Asp/Glu)-His-nucleophile triad found in serine proteases (*1*), phosphatidylinositol-specific phospholipase C (*57*), cholinesterases (*58*, *59*), and hydroxynitrile lyase (*60*). In each case, the bridging His $N^{\epsilon2}$ is close to the activated nucleophile, which can be Ser, Glu, Asp, or part of a substrate, while the $N^{\delta1}$ forms a strong hydrogen bond to the carboxyl group of a second Glu or Asp. This latter interaction, best described as a short ionic hydrogen bond (*61*), rather than a low-barrier hydrogen bond (*62*), typically leads to a HX-protected His $H^{\delta1}$ with a diagnostic downfield resonance. Recent quantum mechanical calculations (*63*, *64*) demonstrated that these downfield proton chemical shifts are a consequence of lengthening of the $N^{\delta1}-H^{\delta1}$ bond, combined with its polarization due to hydrogen bonding to a negatively charged carboxyl in the catalytic triad. Consistent with these calculations, the most downfield-shifted NMR signals in CexCD appear to arise from $^1H^{\delta1}-^{15}N^{\delta1}$ or $^1H^{\epsilon2}-^{15}N^{\epsilon2}$ pairs involved in hydrogen bonds with negatively charged carboxylate acceptors (i.e., His107-Glu53; Figure 8A and Table S1 of the Supporting Information). Furthermore, the $^1H^{\epsilon2}$ and $^{15}N^{\epsilon2}$ atoms of His205 are unusually upfield shifted in 2FCb-CexCD, where its hydrogen bond acceptor Glu233 is neutralized in a glycosidic linkage, yet more typically downfield in apo-CexCD, XbIm·CexCD, and XbIso·CexCD where Glu233 most likely remains negatively charged. Interestingly, the $^1H^{\delta1}$ and $^{15}N^{\delta1}$ chemical shifts of His80 in inhibited 2FCb-CexCD are also relatively upfield, which by this argument is indicative of hydrogen bonding to Asp123 in its neutral state, as hypothesized above.

Histidine $^1J_{NH}$ Coupling Constants

To characterize further the histidines in CexCD, we attempted to measure $^{3h}J_{NC}$ coupling constants between the imidazole $^{15}N^{\delta1/\epsilon2}$ and the side chain carboxyl $^{13}C^{\gamma/\delta}$ of their Asp/Glu hydrogen bond partners. These $^{3h}J_{NC}$ values are related to the covalent character of the hydrogen bond and the N−O distance (*65*). Unfortunately, the short ^{15}N transverse relaxation times of this 34 kDa ^{2}H-, ^{13}C-, and ^{15}N-

labeled protein precluded these measurements. However, as a function of both N−H (*66*) and donor−acceptor distances (*67*), the more easily determined $^1J_{NH}$ coupling constants also provide insights into the nature of a hydrogen bond.

The observed $^1J_{HN}$ coupling constants of the histidines in CexCD vary from ∼85 to 100 Hz and show an inverse correlation with their $^{15}N^{\delta1/\epsilon2}$ (Figure 8b) and $^1H^{\delta1/\epsilon2}$ (not shown) chemical shifts. Similar correlations were found for the OHN hydrogen bonds of pyridine acid complexes (*68*) and the NHN hydrogen bonds of DNA (*69*). This correlation is consistent with the above-mentioned quantum mechanical calculations (*64*), attributing a downfield ^1H chemical shift to the lengthening of the N−H bond, which in turn leads to a smaller $^1J_{NH}$ coupling constant (*66*). This is most readily seen with His107, where the downfield-shifted $^1H^{\delta1}-^{15}N^{\delta1}$, which hydrogen bonds to Glu52, has a $^1J_{NH}$ significantly smaller than that of the upfield-shifted $^1H^{\epsilon2}-^{15}N^{\epsilon2}$, which hydrogen bonds to a buried water [∼91 Hz vs ∼99 Hz (Table S1 of the Supporting Information)].

Concluding Remarks

By providing residue-specific pK_a values, NMR spectroscopy can yield detailed insights into the electrostatic bases for enzymatic catalysis. Through steady advances in NMR instrumentation and methodology, it is now possible to investigate in detail higher-molecular weight systems, such as the 34 kDa catalytic domain of Cex. The pK_a values of the five histidines within this protein range from <2.3 to >10.4 and can change by more than 5 log units upon formation of the glycosyl−enzyme intermediate, thus reflecting their distinct environments and functional roles. We speculate that the potential for complex structural and electrostatic interactions increases with larger proteins and protein complexes, including those associated with membranes, and thus, a similar, if not greater, range of pK_a values may exist for their constituent ionizable groups. A continuing challenge will be to experimentally and theoretically dissect the factors that establish these critical electrostatic interactions and to understand their roles in biological processes such as enzymatic catalysis. Systems of the complexity of CexCD are now entering the realm of accessibility to quantum mechanical electrostatic calculations, and thus, detailed, site-specific measurements of the type presented here, along with high-resolution X-ray or neutron crystallographic structures, will be of particular value in benchmarking such efforts.

ACKNOWLEDGMENT

We thank Wing-Yiu Choy, Lewis Kay, Gregory Lee, Ranjith Muhandiram, and Mark Okon for assistance with NMR spectroscopy, Martin Ludwiczek for help with cloning, Spencer Williams for providing inhibitors, Shouming He for mass spectrometric analyses, and Ibon Alkorta, Jan Jensen, and Ilja Shenderovich for helpful discussions.

SUPPORTING INFORMATION AVAILABLE

Chemical shifts and $^1J_{NH}$ couplings (Table S1) and predicted pK_a values (Table S2) for the histidine residues in apo-CexCD and inhibited CexCD. This material is available free of charge via the Internet at http://pubs.acs.org.

REFERENCES

1. Bachovchin, W. W. (2001) Contributions of NMR spectroscopy to the study of hydrogen bonds in serine protease active sites, *Magn. Reson. Chem. 39*, S199−S213.
2. O'Neill, G., Goh, S. H., Warren, R. A., Kilburn, D. G., and Miller, R. C., Jr. (1986) Structure of the gene encoding the exoglucanase of *Cellulomonas fimi*, *Gene 44*, 325−330.
3. Poon, D. K., Withers, S. G., and McIntosh, L. P. (2006) Direct demonstration of the flexibility of the glycosylated proline-threonine linker in the *Cellulomonas fimi* xylanase Cex through NMR spectroscopic analysis, *J. Biol. Chem. 282*, 2091−2100.
4. Notenboom, V., Birsan, C., Warren, R. A. J., Withers, S. G., and Rose, D. R. (1998) Exploring the cellulose/xylan specificity of the β-1,4-glycanase Cex from *Cellulomonas fimi* through crystallography and mutation, *Biochemistry 37*, 4751−4758.
5. White, A., Tull, D., Johns, K., Withers, S. G., and Rose, D. R. (1996) Crystallographic observation of a covalent catalytic intermediate in a β-glycosidase, *Nat. Struct. Biol. 3*, 149−154.
6. Coutinho, P. M., and Henrissat, B. (1999) Carbohydrate-active enzymes: An integrated database approach, in *Recent Advances in Carbohydrate Bioengineering* (Gilbert, H. J., Davies, G., Henrissat, B., and Svensson, B., Eds.) pp 3−12, The Royal Society of Chemistry, London.
7. Rye, C. S., and Withers, S. G. (2000) Glycosidase mechanisms, *Curr. Opin. Chem. Biol. 4*, 573−580.
8. Tull, D., and Withers, S. G. (1994) Mechanisms of cellulases and xylanases: A detailed kinetic study of the exo-β-1,4-glycanase from *Cellulomonas fimi*, *Biochemistry 33*, 6363−6370.
9. MacLeod, A. M., Lindhorst, T., Withers, S. G., and Warren, R. A. J. (1994) The acid/base catalyst in the exoglucanase/xylanase from *Cellulomonas fimi* is glutamic acid 127: Evidence from detailed kinetic studies on mutants, *Biochemistry 33*, 6571−6376.
10. Notenboom, V., Williams, S. J., Hoos, R., Withers, S. G., and Rose, D. R. (2000) Detailed structural analysis of glycosidase/inhibitor interactions: Complexes of Cex from *Cellulomonas fimi* with xylobiose-derived aza-sugars, *Biochemistry 39*, 11553−11563.
11. Williams, S. J., Hoos, R., and Withers, S. G. (2000) Nanomolar versus millimolar inhibition by xylobiose-derived azasugars: Significant differences between two structurally distinct xylanases, *J. Am. Chem. Soc. 122*, 2223−2235.
12. Poon, D. K. Y., Ludwiczek, M. L., Schubert, M., Kwan, E. M., Withers, S. G., and McIntosh, L. P. (2007) NMR spectroscopic characterization of a β-(1,4)-glycosidase along its reaction pathway: Stabilization upon formation of the glycosyl-enzyme intermediate, *Biochemistry 46*, 1759−1770.
13. Muchmore, D. C., McIntosh, L. P., Russell, C. B., Anderson, D. E., and Dahlquist, F. W. (1989) Expression and nitrogen-15 labeling of proteins for proton and nitrogen-15 nuclear magnetic resonance, *Methods Enzymol. 177*, 44−73.
14. Delaglio, F., Grzesiek, S., Vuister, G. W., Zhu, G., Pfeifer, J., and Bax, A. (1995) NMRPipe: A multidimensional spectral processing system based on UNIX pipes, *J. Biomol. NMR 6*, 277−293.
15. Goddard, T. D., and Kneeler, D. G. (1999) *Sparky 3*, 3rd ed., University of California, San Francisco.
16. Wishart, D. S., Bigam, C. G., Yao, J., Abildgaard, F., Dyson, H. J., Oldfield, E., Markley, J. L., and Sykes, B. D. (1995) ^1H, ^{13}C and ^{15}N chemical shift referencing in biomolecular NMR, *J. Biomol. NMR 6*, 135−140.
17. Sklenár, V., and Bax, A. (1987) Spin-echo water suppression for the generation of pure-phase two-dimensional NMR spectra, *J. Magn. Reson. 74*, 469−479.
18. Kay, L. E., Keifer, P., and Saarinen, T. (1992) Pure absorption gradient enhanced heteronuclear single quantum correlation spectroscopy with improved sensitivity, *J. Am. Chem. Soc. 114*, 10663−10665.
19. Singer, A. U., and Forman-Kay, J. D. (1997) pH titration studies of an SH2 domain-phosphopeptide complex: Unusual histidine and phosphate pKa values, *Protein Sci. 6*, 1910−1919.
20. Santoro, J., and King, G. C. (1992) A constant-time 2D Overbodenhausen experiment for inverse correlation of isotopically enriched species, *J. Magn. Reson. 97*, 202−207.
21. Mulder, F. A. A., Spronk, C., Slijper, M., Kaptein, R., and Boelens, R. (1996) Improved HSQC experiments for the observation of exchange broadened signals, *J. Biomol. NMR 8*, 223−228.
22. Yamazaki, T., Forman-Kay, J. D., and Kay, L. E. (1993) NMR experiments for correlating $^{13}C\beta$ and $^1H\delta/\epsilon$ chemical shifts of

aromatic residues in ^{13}C-labelled proteins via scalar couplings, *J. Am. Chem. Soc. 115*, 11054−11055.
23. Slupsky, C. M., Gentile, L. N., and McIntosh, L. P. (1998) Assigning the NMR spectra of aromatic amino acids in proteins: Analysis of two ETS pointed domains, *Biochem. Cell Biol. 76*, 379−390.
24. Ottiger, M., Delaglio, F., and Bax, A. (1998) Measurement of J and dipolar couplings from simplified two-dimensional NRM spectra, *J. Magn. Reson. 131*, 373−378.
25. Connelly, G. P., and McIntosh, L. P. (1998) Characterization of a buried neutral histidine in *Bacillus circulans* xylanase: Internal dynamics and interaction with a bound water molecule, *Biochemistry 37*, 1810−1818.
26. Hwang, T.-L., van Zijl, P. C. M., and Mori, S. (1998) Accurate quantitation of water-amide proton exchange rates using the phase-modulated CLEAN chemical EXchange (CLEANEX-PM) approach with a fast-HSQC (FHSQC) detection scheme, *J. Biomol. NMR 11*, 221−226.
27. Joshi, M. D., Sidhu, G., Nielsen, J. E., Brayer, G. D., Withers, S. G., and McIntosh, L. P. (2001) Dissecting the electrostatic interactions and pH-dependent activity of a family 11 glycosidase, *Biochemistry 40*, 10115−10139.
28. Notenboom, V., Birsan, C., Nitz, M., Rose, D. R., Warren, R. A. J., and Withers, S. G. (1998) Insights into transition state stabilization of the β-1,4-glycosidase Cex by covalent intermediate accumulation in active site mutants, *Nat. Struct. Biol. 5*, 812−818.
29. Pelton, J. G., Torchia, D. A., Meadow, N. D., and Roseman, S. (1993) Tautomeric states of the active-site histindines of phosphorylated and unphosphorylated IIIGlc, a signal-transducing protein from *Escherichia coli*, using two-dimensional heteronuclear NMR techniques, *Protein Sci. 2*, 543−558.
30. Gloster, T., Williams, S. J., Tarling, C. A., Roberts, S., Dupont, C., Jodoin, P., Shareck, F., Withers, S. G., and Davies, G. J. (2003) A xylobiose-derived isofagomine lactam glycosidase inhibitor binds as its amide tautomer, *Chem. Commun.*, 944−945.
31. Bax, A., and Marion, D. (1988) Improved resolution and sensitivity in ^{1}H-detected heteronuclear multiple-bond correlation spectroscopy, *J. Magn. Reson. 78*, 186−191.
32. Sudmeier, J., Bradshaw, E., Haddad, K., Day, R., Thalhauser, C., Bullock, P., and Bachovchin, W. (2003) Identification of histidine tautomers in proteins by 2D ^{1}H/$^{13}C^{\delta 2}$ one-bond correlated NMR, *J. Am. Chem. Soc. 125*, 8430−8431.
33. Plesniak, L. A., Connelly, G. P., Wakarchuk, W. W., and McIntosh, L. P. (1996) Characterization of a buried neutral histidine residue in *Bacillus circulans* xylanase: NMR assignments, pH titration, and hydrogen exchange, *Protein Sci. 5*, 2319−2328.
34. Kaslik, G., Westler, W. M., Graf, L., and Markley, J. L. (1999) Properties of the His57-Asp102 dyad of rat trypsin D189S in the zymogen, activated enzyme, and α1-proteinase inhibitor complexed forms, *Arch. Biochem. Biophys. 262*, 254−264.
35. Yu, L., and Fesik, S. W. (1994) pH titration of the histidine residues of cyclophilin and FK506 binding protein in the absence and presence of immunosuppressant ligands, *Biochim. Biophys. Acta 1209*, 24−32.
36. Lui, T., Ryan, M., Dahlquist, F. W., and Griffith, O. H. (1997) Determination of the pK_a values of the histidine side chains of phosphatidylinositol-specific phosholipase C from *Bacillus cereus* by NMR spectroscopy and site-directed mutagenesis, *Protein Sci. 6*, 1937−1944.
37. Blomberg, F., Maurer, W., and Rüterjans, H. (1977) Nuclear magnetic resonance investigation of ^{15}N-labeled histidine in aqueous solution, *J. Am. Chem. Soc. 99*, 8149−8159.
38. Bundi, A., and Wüthrich, K. (1979) ^{1}H-NMR parameters of the common amino acid residues measured in aqueous solutions of the linear tetrapeptides H-Gly-Gly-X-L-Ala-OH, *Biopolymers 18*, 285−297.
39. Richarz, R., and Wuthrich, K. (1978) Carbon-13 NMR chemical shifts of the common amino acid residues measured in aqueous solutions of the linear tetrapeptides H-Gly-Gly-X-L-Ala-OH, *Biopolymers 17*, 2133−2141.
40. Bachovchin, W. W., and Roberts, J. D. (1978) N-15 nuclear magnetic-resonance spectroscopy: State of histidine in catalytic triad of α-lytic protease: Implications for charge-relay mechanism of peptide-bond cleavage by serine proteases, *J. Am. Chem. Soc. 100*, 8041−8047.
41. Joshi, M. D., Hedberg, A., and McIntosh, L. P. (1997) Complete measurement of the pK_a values of the carboxyl and imidazole groups in *Bacillus circulans* xylanase, *Protein Sci. 6*, 2667−2670.
42. Edgcomb, S. P., and Murphy, K. P. (2002) Variability in the pKa of histidine side-chains correlates with burial within proteins, *Proteins 49*, 1−6.
43. Varrot, A., Tarling, C. A., Macdonald, J. M., Stick, R. V., Zechel, D. L., Withers, S. G., and Davies, G. J. (2003) Direct observation of the protonation state of an imino sugar glycosidase inhibitor upon binding, *J. Am. Chem. Soc. 125*, 7496−7497.
44. Poon, D. K., Schubert, M., Au, J., Okon, M., Withers, S. G., and McIntosh, L. P. (2006) Unambiguous determination of the ionization state of a glycoside hydrolase active site lysine by ^{1}H-^{15}N heteronuclear correlation spectroscopy, *J. Am. Chem. Soc. 128*, 15388−15389.
45. Anderson, D. E., Becktel, W. J., and Dahlquist, F. W. (1990) pH-induced denaturation of proteins: A single salt bridge contributes 3−5 kcal/mol to the free energy of folding of T4 lysozyme, *Biochemistry 29*, 2403−2408.
46. Wicki, J., Schloegl, J., Tarling, C. A., and Withers, S. G. (2007) Recruitment of both uniform and differential binding energy in enzymatic catalysis: Xylanases from Families 10 and 11, *Biochemistry* (in press).
47. McIntosh, L. P., Hand, G., Johnson, P. E., Joshi, M. D., Korner, M., Plesniak, L. A., Ziser, L., Wakarchuk, W. W., and Withers, S. G. (1996) The pK_a of the general acid/base carboxyl group of a glycosidase cycles during catalysis: A ^{13}C-NMR study of *Bacillus circulans* xylanase, *Biochemistry 35*, 9958−9966.
48. Varrot, A., Schulein, M., Pipelier, M., Vasella, A., and Davies, G. J. (1999) Lateral protonation of a glycosidase inhibitor. Structure of the *Bacillus agaradhaerens* Cel5A in complex with a cellobiose-derived imidazole at 0.97 Å resolution, *J. Am. Chem. Soc. 121*, 2621−2622.
49. Gloster, T. M., Roberts, S., Perugino, G., Rossi, M., Moracci, M., Panday, N., Terinek, M., Vasella, A., and Davies, G. J. (2006) Structural, kinetic, and thermodynamic analysis of glucoimidazole-derived glycosidase inhibitors, *Biochemistry 45*, 11879−11884.
50. Zechel, D. L., Boraston, A. B., Gloster, T., Boraston, C. M., Macdonald, J. M., Tilbrook, D. M. G., Stick, R. V., and Davies, G. J. (2003) Iminosugar glycosidase inhibitors: Structural and thermodynamic dissection of the binding of isofagomine and 1-deoxynojirimycin to β-glucosidases, *J. Am. Chem. Soc. 125*, 14313−14323.
51. Betz, M., Lohr, F., Wienk, H., and Ruterjans, H. (2004) Long-range nature of the interactions between titratable groups in *Bacillus agaradhaerens* family 11 xylanase: pH titration of *B. agaradhaerens* xylanase, *Biochemistry 43*, 5820−5831.
52. Day, R. M., Thalhauser, C. J., Sudmeier, J. L., Vincent, M. P., Torchilin, E. V., Sanford, D. G., Bachovchin, C. W., and Bachovchin, W. W. (2003) Tautomerism, acid-base equilibria, and H-bonding of the six histidines in subtilisin BPN′ by NMR, *Protein Sci. 12*, 794−810.
53. Stoesz, J. D., Malinowski, D. P., and Redfield, A. G. (1979) Nuclear magnetic resonance study of solvent exchange and nuclear Overhauser effect of the histidine protons of bovine superoxide dismutase, *Biochemistry 18*, 4669−4675.
54. Nielsen, J. E., and Vriend, G. (2001) Optimizing the hydrogen-bond network in Poisson-Boltzmann equation-based pK_a calculations, *Proteins 43*, 403−412.
55. Li, H., Robertson, A. D., and Jensen, J. H. (2005) Very fast empirical prediction and interpretation of protein pKa values, *Proteins 61*, 704−721.
56. Farr-Jones, S., Wong, W. Y. L., Gutheil, W. G., and Bachovchin, W. W. (1993) Direct observation of the tautomeric forms of histidine in N-15 NMR-spectra at low-temperatures: Comments on intramolecular hydrogen-bonding and on tautomeric equilibrium-constants, *J. Am. Chem. Soc. 115*, 6813−6819.
57. Ryan, M., Liu, T., Dahlquist, F. W., and Griffith, O. H. (2001) A catalytic diad involved in substrate-assisted catalysis: NMR study of hydrogen bonding and dynamics at the active site of phosphatidylinositol-specific phospholipase C, *Biochemistry 40*, 9743−9750.
58. Viragh, C., Harris, T. K., Reddy, P. M., Massiah, M. A., Mildvan, A. S., and Kovach, I. M. (2000) NMR evidence for a short, strong hydrogen bond at the active site of a cholinesterase, *Biochemistry 39*, 16200−16205.
59. Massiah, M. A., Viragh, C., Reddy, P. M., Kovach, I. M., Johnson, J., Rosenberry, T. L., and Mildvan, A. S. (2001) Short, strong hydrogen bonds at the active site of human acetylcholinesterase: Proton NMR studies, *Biochemistry 40*, 5682−5690.
60. Stranzl, G. R., Gruber, K., Steinkellner, G., Zangger, K., Schwab, H., and Kratky, C. (2004) Observation of a short, strong hydrogen

bond in the active site of hydroxynitrile lyase from *Hevea brasiliensis* explains a large pKa shift of the catalytic base induced by the reaction intermediate, *J. Biol. Chem. 279*, 3699−3707.
61. Fuhrmann, C. N., Daugherty, M. D., and Agard, D. A. (2006) Sub-angstrom crystallography reveals that short ionic hydrogen bonds, and not a His-Asp low-barrier hydrogen bond, stabilize the transition state in serine protease catalysis, *J. Am. Chem. Soc. 128*, 9086−9102.
62. Frey, P. A. (2001) Strong hydrogen bonding in molecules and enzymatic complexes, *Magn. Reson. Chem. 39*, S190−S198.
63. Westler, W. M., Weinhold, F., and Markley, J. L. (2002) Quantum chemical calculations on structural models of the catalytic site of chymotrypsin: Comparison of calculated results with experimental data from NMR spectroscopy, *J. Am. Chem. Soc. 124*, 14373−14381.
64. Molina, P. A., Sikorski, R. S., and Jensen, J. H. (2003) NMR chemical shifts in the low-pH form of α-chymotrypsin. A QM/MM and ONIOM-NMR study, *Theor. Chem. Acc. 109*, 100−107.
65. Cornilescu, G., Hu, J. S., and Bax, A. (1999) Identification of the hydrogen bonding network in a protein by scalar couplings, *J. Am. Chem. Soc. 121*, 2949−2950.
66. Tuttle, T., Kraka, E., Wu, A., and Cremer, D. (2004) Investigation of the NMR spin-spin coupling constants across the hydrogen bonds in ubiquitin: The nature of the hydrogen bond as reflected by the coupling mechanism, *J. Am. Chem. Soc. 126*, 5093−5107.
67. Barfield, M., Dingley, A. J., Feigon, J., and Grzesiek, S. (2001) A DFT study of the interresidue dependencies of scalar J-coupling and magnetic shielding in the hydrogen-bonding regions of a DNA triplex, *J. Am. Chem. Soc. 123*, 4014−4022.
68. Limbach, H. H., Pietrzak, M., Sharif, S., Tolstoy, P. M., Shenderovich, I. G., Smirnov, S. N., Golubev, N. S., and Denisov, G. S. (2004) NMR parameters and geometries of OHN and ODN hydrogen bonds of pyridine-acid complexes, *Chem.−Eur. J. 10*, 5195−5204.
69. Dingley, A. J., Masse, J. E., Peterson, R. D., Barfield, M., Feigon, J., and Grzesiek, S. (1999) Internucleotide scalar couplings across hydrogen bonds in Watson-Crick and Hoogsteen base pairs of a DNA triplex, *J. Am. Chem. Soc. 121*, 6019−6027.
70. Koradi, R., Billeter, M., and Wüthrich, K. (1996) MOLMOL: A program for display and analysis of macromolecular structures, *J. Mol. Graphics 14*, 51−55, 29−32.

BI700249M